PCCP



View Article Online **PAPER**



Cite this: Phys. Chem. Chem. Phys., 2020, 22, 23141

Received 22nd June 2020, Accepted 16th September 2020

DOI: 10.1039/d0cp03333b

rsc.li/pccp

Resonant states in cyanogen NCCN†

Pamir Nag, 📭 a Roman Čurík, * a Michal Tarana, a Miroslav Polášek, a

In a combined experimental and theoretical study we probe the transient anion states (resonances) in cyanogen. Experimentally, we utilize electron energy loss spectroscopy which reveals the resonance positions by monitoring the excitation functions for vibrationally inelastic electron scattering. Four resonances are visible in the spectra, centered around 0.36 eV, 4.1, 5.3 and 7.3 eV. Theoretically, we explore the resonant states by using the regularized analytical continuation method. A very good agreement with the experiment is obtained for low-lying resonances, however, the computational method becomes unstable for higher-lying states. The lowest shape resonance $({}^{2}\Pi_{IJ})$ is independently explored by the complex adsorbing potential method. In the experiment, this resonance is manifested by a pronounced boomerang structure. We show that the naive picture of viewing NCCN as a pseudodihalogen and focusing only on the CC stretch is invalid.

1 Introduction

Astronomical observations report that neutral cyanopolyacetylenes and nitriles occur abundantly in space and in planetary atmospheres.^{1,2} The electronic structure of these compounds has been largely probed by laboratory experiments and theoretical methods. However, there is a clear imbalance in the amount of available information about the neutral and cationic species on one hand, and anions on the other hand. This has been slowly changing, and in recent years more and more attention shifted to the negative species^{3,4} primarily motivated by two facts: first, the linear species CN-, C₃N-, and C₅N- were among the first molecular anions detected in outer space.5,6 Second, CN- has a high abundance in the atmosphere of Titan and can lead to the production of large anionic species observed there.7,8

In the present study we focus on the simplest cyanopolyyne, cyanogen NCCN. Neutral cyanogen has been identified in Titan's atmosphere.9 Its direct spectroscopic identification in outer space is challenging due to its lack of polarity, but its presence is strongly supported by the detection of protonated cyanogen (NCCNH⁺)¹⁰ and its polar isomer isocyanogen (CNCN).² NCCN is then one of the possible precursors of the CN⁻ anion in the

Electronically bound anions of various cyanogen isomers were theoretically explored by Nsangou et al. 11 Here we investigate electronic states embedded in the continuum (resonances). These short-lived states were previously experimentally probed by electron transmission spectroscopy¹² and by dissociative electron attachment spectroscopy. 13-15 Theoretically, Sebastianelli and Gianturco 16 carried out single-center expansion scattering calculations, and Michelin et al. 17 computed integral scattering cross sections with the Schwinger variational method.

Our experimental tool is electron energy loss spectroscopy. The resonances formed in electron collisions with a target molecule typically lead to an enhancement of vibrational excitation cross sections. Monitoring excitation functions of the individual vibrational modes is thus a sensitive probe for the formation of transient

In order to interpret the data, we explore the continuum states by two theoretical approaches, the regularized analytic continuation (RAC) method and the complex adsorbing potential (CAP) method. Using the latter method, we also construct a local diatomic-like model for the CC stretch excitation via the lowest shape resonance. It is shown that this "pseudodihalogen" model is too drastic a simplification to reproduce the oscillatory structures visible in the measured cross section.

^a J. Heyrovský Institute of Physical Chemistry, Czech Academy of Sciences, Dolejškova 3, 18223 Prague, Czech Republic. E-mail: roman.curik@jh-inst.cas.cz, juraj.fedor@jh-inst.cas.cz

2 Experimental methods and results

The cyanogen sample was prepared by a modified literature procedure¹⁸ in which an aqueous solution of potassium cyanide (11.6 g in 50 ml of water) was poured onto 22.3 g of copper(II)

astro-environments which motivates our interest in its anion chemistry.

^b SOKENDAI, The Graduate University for Advanced Studies, Nishigonaka, Myodaiji, Okazaki 444-8585, Japan

^c Department of Chemistry and Physics, Southeastern Louisiana University, SLU 10878, Hammond, LA 70402, USA. E-mail: thomas.sommerfeld@selu.edu † Electronic supplementary information (ESI) available. See DOI: 10.1039/

PCCP Paper

sulphate pentahydrate powder at a temperature rising from 50 °C to 90 °C. Evolving cyanogen was passed through a Dimroth condenser to remove the water vapor. Then it was captured in a flask cooled down by a mixture of dry ice and acetone to a temperature of -78 °C. Subsequently, the frozen cyanogen was resublimed under vacuum (<1 mbar) into a lecture bottle. Its purity was checked by electron-impact mass spectrometry and determined to be better than 98%.

The electron scattering measurements were performed on the electrostatic electron energy loss spectrometer with a hemispherical monochromator and an analyser. All the present data were recorded at a fixed scattering angle of 135°. The resolution was around 18 meV in the energy loss mode. The energy of the incident beam was calibrated on the 19.365 eV He⁻(²S) resonance. The absolute elastic cross section was determined by the relative flow method using helium as the calibration gas. The elastic cross section is accurate within $\pm 15\%$. The vibrationally inelastic cross sections were calibrated against the elastic cross section. They have only indicative absolute values - as will be seen, the individual energy loss peaks are not fully resolved. For the overlapping peaks, we did not attempt to fit the individual contributions.

In the experiment, the vibrational modes of neutral cyanogen are excited. The frequencies of these modes are known from optical spectroscopy¹⁹ and listed in Table 1 (the bending modes are doubly degenerate). Fig. 1 shows electron energy loss spectra at four different incident energies. In this type of measurement, the incident energy E_i is kept fixed and the residual energy of the scattered electrons $E_{\rm r}$ is scanned. The signal is plotted as a function of the electron energy loss $\Delta E = E_i - E_r$. The peak at 0 eV energy loss thus corresponds to elastic scattering, while the peaks at higher energy losses are related to the excitation of specific vibrations. All the normal modes are visible in the spectra (with different relative intensities at different energies), apart from the v_3 CN asymmetric stretch excitation which is practically invisible in our spectra.

The spectrum shown in the top panel of Fig. 1 (incident energy of 0.365 eV) shows a large peak at the incident energy (right-most peak). This peak corresponds to 100% conversion of the incident energy to internal energy of the molecule, and emission of electrons with very low residual energies. Such strong electron thermalization has been observed in a number of molecules. 20-22

Fig. 2 shows the excitation curves of three various energy losses. Here, the incident energy $E_{\rm i}$ and the residual energy $E_{\rm r}$ are scanned synchronously keeping the energy loss ΔE constant. Zero energy loss ($\Delta E = 0$ eV, top panel) corresponds to

Table 1 Experimental vibrational frequencies of NCCN from ref. 19

Label	Mode description	Energy (meV)
$\overline{\nu_1}$	CN sym. stretch	288
ν_2	CC stretch	105
ν_3	CN asym. stretch	267
$ u_4$	Asym. bend	62
ν_5	Sym. bend	29

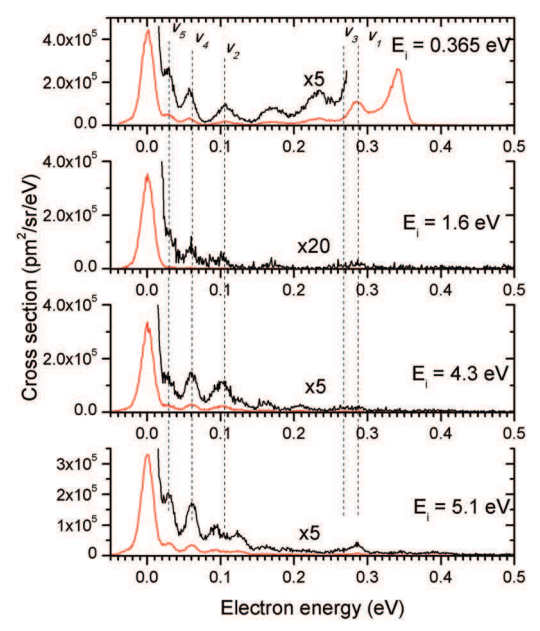


Fig. 1 Electron energy loss spectra of cyanogen recorded at four different incident electron energies.

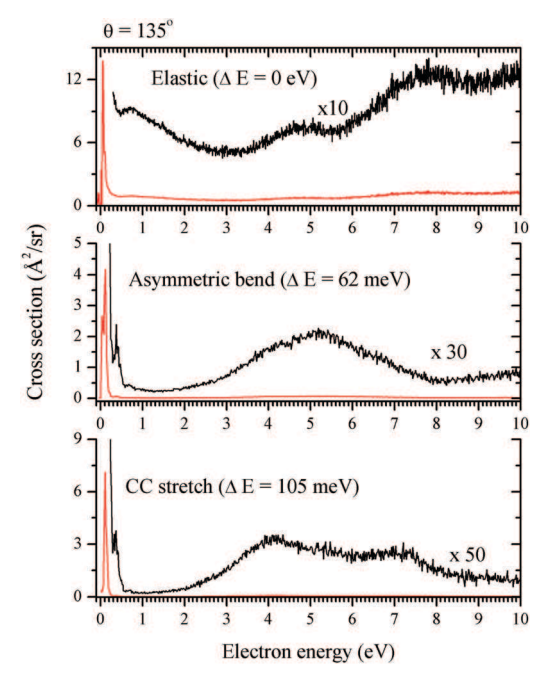


Fig. 2 Excitation curves of three different energy losses, corresponding to elastic scattering and the excitation of the asymmetric bend and CC stretch.

elastic scattering. The elastic cross section shows a steep rise at very low electron energies, and then a number of broad oscillatory features. The other two panels of Fig. 2 show excitation functions of the asymmetric bend v_4 and CC stretch v_2 . These modes were chosen since the energy loss spectra in Fig. 1 indicated their strong excitation at high incident energies. Both show a strong threshold peak and a sharp resonance around 0.36 eV. This resonance shows a pronounced boomerang structure which will

PCCP

be discussed in Section 4. At higher electron energies, the behavior of the v_4 and v_2 excitation curves is very different. The bending mode shows a maximum around 5.3 eV, and the CC stretch mode shows two maxima at 4.1 and 7.3 eV.

Jordan and co-workers¹² recorded the transmission electron spectrum (ETS) of NCCN and saw two resonances, centered around 0.58 eV and 5.37 eV, in very good agreement with the present data (the exact position of the lowest resonance is difficult to determine due to the oscillatory character of the vibrational structure, see the discussion at the beginning of Section 4). They assigned these to the formation of ${}^{2}\Pi_{11}$ and ${}^{2}\Pi_{22}$ states, respectively. Based on the virtual orbital ordering, they concluded that there should be two other σ^* shape resonances, $^{2}\Sigma_{\rm u}$ lying between the π^{*} states, $^{2}\Sigma_{\rm g}$ lying above $^{2}\Pi_{\rm g}$. Jordan and co-workers concluded that these are too broad (i.e. they have very short lifetimes) to be discerned in a total cross-section measurement such as ETS. In contrast, the present excitation cross sections not only reveal the Σ resonances, but, in addition, show the propensity of each resonance for exciting certain normal modes. Formation of the ${}^2\Pi_{\rm g}$ transient state at 5.3 eV leads to strong excitation of the asymmetric bending mode, but it does not lead to any considerable excitation of the CC stretch. On the other hand, both Σ states are clearly visible in the CC stretch excitation, similarly as in other polyynes probed previously. 23,24

3 RAC calculations of resonances in **NCCN**

The regularized analytic continuation (RAC)^{25,26} belongs to the class of methods called analytic continuation in coupling constant (ACCC). 27-30 The ACCC methods introduce an attractive perturbation potential V to the molecular Hamiltonian H,

$$H \to H + \lambda V$$
, (1)

for calculations of electron affinities. The attractive force λV transfers the resonant state into a bound state making the problem amenable for standard quantum chemistry calculations. Different choices of the perturbation potential V were explored previously.31-33 In the present study we employ oneelectron operator represented by Coulomb potential distributed evenly over all the four nuclei

$$\lambda V(\vec{r}) = \sum_{d=1}^{4} \frac{\lambda}{|\vec{r} - \vec{R}_{\rm A}|},\tag{2}$$

where \vec{R}_A are positions of the two carbon and the two nitrogen atoms.

Electron affinities in the presence of the perturbation potential (2) were computed by the CCSD(T) method^{34,35} as implemented in the MOLPRO 2010 package of quantum chemistry programs.³⁶ Dunning's correlation-consistent quadruple-zeta basis was used³⁷ (cc-pVQZ) to compute all affinities analyzed by the RAC method, and an example for three typical affinity curves $\Delta E(\lambda)$ = $\kappa^2(\lambda)$ is shown in Fig. 3 for the lowest three resonant states detected at the equilibrium geometry. Each of the curves shown in Fig. 3 contains abound 120-150 data points.

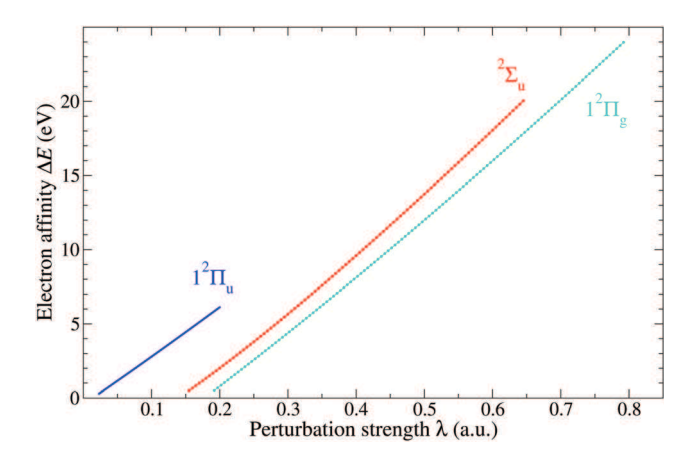


Fig. 3 Computed vertical electron affinities $\Delta E(\lambda)$ for the lowest three resonant states observed computationally at the equilibrium geometry. In the case of the $1^2\Pi_u$ resonance, the high number of data points (150) displays as a smooth thick line.

We note that while augmentation of the valence basis set with diffuse functions is normally needed when dealing with anions, the additional attractive potential λV used in the RAC method ensures that the excess electron is bound and that the computed affinities have substantial values (see Fig. 3). Thus, the basis set is only needed to describe compact wave functions and helps, in fact, to eliminate weakly bound Rydberg states that could be supported in the perturbation field (cf. analysis in 2).

The RAC method²⁵ is based on the inverse variant of the more general ACCC approach. In the present study the RAC [3/1] Padé approximation²⁶ was employed for the function $\lambda(\kappa)$:

$$\lambda^{[3/1]}(\kappa) = \lambda_0 \frac{\left(\kappa^2 + 2\alpha^2\kappa + \alpha^4 + \beta^2\right)\left(1 + \delta^2\kappa\right)}{\alpha^4 + \beta^2 + \kappa(2\alpha^2 + \delta^2(\alpha^4 + \beta^2))},\tag{3}$$

where λ_0 , α , β , and δ are the fitting parameters yielding the resonance energy $E_{\rm r} = \beta^2 - \alpha^4$ and the resonance width $\Gamma = 4\alpha^2 |\beta|$.

Potential energy curves computed along the C-C bond distance are shown in Fig. 4. The molecule is kept at a linear geometry with its C-N bond lengths fixed at the neutral equilibrium value of 1.161 Å. Data shown in Fig. 4 demonstrate that the ${}^{2}\Sigma_{11}$ curve exhibits a minimum around R = 2.3 Å, where *R* denotes the C–C bond length. Gerade and ungerade $^{2}\Sigma$ states become degenerate at larger distances (not shown in Fig. 4), while the degeneracy of the ²Π states is already visible in the displayed data.

Six resonant potential curves explored by the RAC method are shown in Fig. 4. Resonant states $1^2\Pi_u$, $^2\Sigma_u$, and $1^2\Pi_g$ can be identified as shape resonances, while $^2\Sigma_{
m g},\, 2^2\Pi_{
m g},$ and $2^2\Pi_{
m u}$ are core-excited resonances as summarized in Table 2.

In the current context, the RAC method can safely determine the core-excited resonances only in regions close to their crossing with the neutral curve where they have reasonably small energies and widths. For shorter C-C distances these resonances rise steeply in energy and width. The RAC method becomes unstable for such high-lying states (for R < 1.8 Å) and the resonances quickly dissipate into the continuum.

Paper PCCP

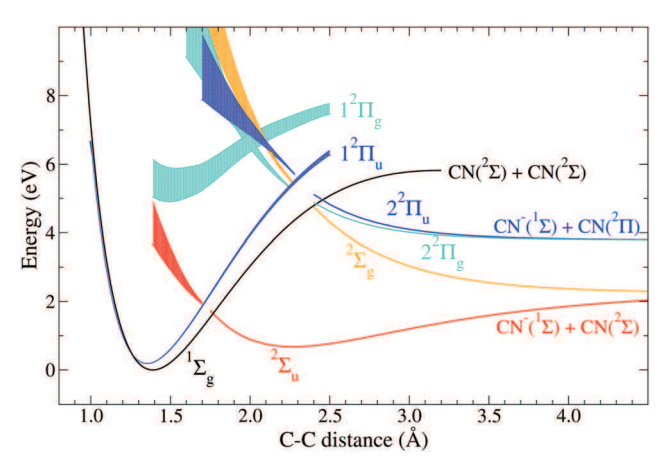


Fig. 4 Potential energy curves along the C–C bond length. The black line shows the dissociation curve of the neutral ground state. Respective anion curves are shown by red $(^2\Sigma_{\rm u})$, orange $(^2\Sigma_{\rm g})$, cyan $(^2\Pi_{\rm g})$, and blue $(^2\Pi_{\rm u})$ lines. Vertical widths of these curves in the autodetachment region correspond to the resonance widths \varGamma .

Table 2 Dominant configuration-state functions (CSFs) for the states presented in Fig. 4. Occupation numbers of the highest occupied orbitals are given for the four symmetries. The fully occupied core $1-4\sigma_g^2$ $1-3\sigma_u^2$ is not listed in the table

	Dominant CSFs								
State	$5\sigma_{ m g}$	$1\pi_{\rm u}$	$2\pi_{\rm u}$	$4\sigma_{ m u}$	$5\sigma_{ m u}$	$1\pi_{\rm g}$	$2\pi_{\mathrm{g}}$	Resonance type	
$^{1}\Sigma_{g}$ $^{2}\Sigma_{u}$	2	4	0	2	0	4	0	Neutral target	
$^{2}\Sigma_{u}^{s}$	2	4	0	2	1	4	0	Shape	
$^{2}\Sigma_{\mathrm{g}}^{\mathrm{g}}$ $1^{2}\Pi_{\mathrm{u}}$	1	4	0	2	2	4	0	Core-excited	
$1^2\Pi_{\rm u}$	2	4	1	2	0	4	0	Shape	
$2^2\Pi_{\rm H}$	2	3	0	2	2	4	0	Core-excited	
$1^2\Pi_g$	2	4	0	2	0	4	1	Shape	
$2^2\Pi_g^s$	2	4	0	2	2	3	0	Core-excited	

A second limitation of the current RAC method is related to its inherent one-state design, in other words, a much more complicated Padé approximant would be needed to account for two states undergoing a crossing. This limitation is apparent for the two pairs of the Π resonances $1^2\Pi_u$ – $2^2\Pi_u$ and $1^2\Pi_g$ – $2^2\Pi_g$, which should undergo avoided crossings around 2.3 Å and 2.0 Å, respectively. Here, we show a diabatic picture, which can be obtained with the RAC method.

Resonance positions and widths computed at equilibrium geometry are listed in Table 3. The resonance listed at 7.3 eV is clearly visible in the experimental data, however it is not seen by the theory. A resonant state at such high energy is well

Table 3 Positions and widths of the shape resonances at equilibrium C–C distance (ordered by the computed resonance energy)

Resonance	$1^2\Pi_{\mathrm{u}}$	$^2\Sigma_{ m u}$	$1^2\Pi_{ m g}$	$^2\Sigma_{ m g}$
Energy $E_{\rm r}$ (eV)	0.220	4.3	5.6	
Width Γ (eV)	0.006	1.2	1.1^a	_
Expt. E_r (eV)	0.36	4.1	5.3	7.3

 $[^]a$ Unstable continuation, Γ inaccurate.

outside the scope of the RAC method combined with the ground-state method employed here – CCSD(T).

The resonances described theoretically in this section were previously analyzed by quantum scattering calculations. ¹⁶ A single-center expansion with an optical potential was used to describe the electron–molecule interaction. In such a one-particle model only shape resonances are visible as sharp changes in the scattering eigenphases or as peaks in the computed cross sections. The qualitative agreement between the observations made by sebastianelli *et al.* ¹⁶ and the present negative ion curves shown in Fig. 4 is good. A corresponding discussion can be summarized in two points:

- The $1^2\Pi_u$ and $1^2\Pi_g$ shape resonances were reported¹⁶ at 1.34 eV and 7.76 eV, respectively, at somewhat higher energies than observed experimentally or calculated here. Moreover, the authors also explored the behavior of these resonances when the C-C bond length is stretched. They found the resonances not to cross the neutral curve at larger C-C bond distances, in agreement with the curves shown in Fig. 4.
- \bullet No equilibrium resonance parameters are reported in ref. 16 for the $^2\Sigma_u$ resonance. However, the authors report a very low-lying (0.12 eV) resonance of $^2\Sigma_u$ symmetry at a stretched C–C bond length of 1.8 Å that becomes a bound state at even larger C–C bond distances. Our computed $^2\Sigma_u$ resonance shown in Fig. 4 crosses the neutral curve at a C–C bond length of 1.77 Å.

4 One-dimensional model for the CC stretch excitation cross section

Based on the spectra reported in Fig. 1 and 2 of Section 2 as well as on the RAC calculation (Section 3) it is clear that the low-energy $1^2\Pi_u$ resonance possesses a relative long lifetime and accordingly shows pronounced coupling to the vibrational motion of the molecule, which leads in turn to sharp (boomerang) structures in the cross sections. In contrast, the higher-lying resonances possess much shorter lifetimes, the excess electron does not remain trapped on the timescale of the vibrational motion, and the structures in the cross sections are very broad.

A magnification of the threshold region of the ΔE = 105 meV excitation cross section (*cf.* Fig. 2), which clearly shows the boomerang structure due to the $1^2\Pi_u$ resonance, is displayed in Fig. 5. At this low energy the oscillatory structure is superimposed on the threshold peak. We assign the vertical resonance position by approximately subtracting the smooth threshold contribution and choosing then the strongest boomerang peak at 0.36 eV. We caution that this value should be taken with a grain of salt as assigning resonance positions in a broad vibrational structure overlapping with a threshold peak is not straightforward.

In general, modeling the observed vibrational structures requires dynamics on a seven dimensional complex potential energy surface. That seems overambitious as a first step, and we decided to test the drastic assumption of neglecting intermolecular vibrational relaxation (IVR). In other words, we modeled NCCN as a collection of oscillators that remain uncoupled on the timescale of the scattering event so that no energy may be

PCCP Paper

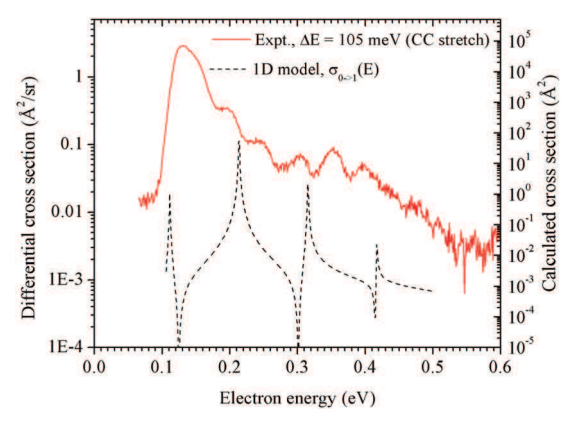


Fig. 5 Red line: experimental differential cross section at 135° for CC stretch excitation. Dashed black line: cross section for vibrational excitation of the CC stretch mode computed with a one-dimensional model (see the ESI†). The vertical scales are arbitrarily shifted.

exchanged between vibrational modes. Then the structures in the ΔE = 105 meV excitation curve (the CC stretching curve in Fig. 2 and 5) can be computed by considering the CC stretch only. In chemical terms, a CN group is a pseudohalogen, and we model NC–CN as a pseudodihalogen.

The detailed implementation of this pseudodihalogen model is described in the ESI,† and the resulting cross section is the dashed line in Fig. 5. However, before discussing the results of the model, let us consider some intermediate results needed to set up the model, namely, typical values of the resonance parameters, $E_{\rm r}$ and Γ , obtained with the CAP method, which can be compared with the RAC results and the experiential assignment of the maximum of the boomerang structure (Table 3).

For the CAP method, we present two pairs of ranges (see Table 4). The first range shows how much the results depend on the choice of equilibrium structure. The experimental gas phase geometry as well as geometries optimized with the B3LYP and CCDT(T) methods and AUG-cc-pVDZ and AUG-ccpVTZ basis sets were considered. Sampling from these geometries, the resonance position is fairly robust, yet the CAP values are somewhat smaller than the RAC value and the experimental center of the boomerang structure. In view of the expected precision of the method, the agreement is satisfactory. Sampling from the same geometries, the width changes by less in absolute terms but by a huge amount in relative terms. The range includes the RAC width.

Table 4 Resonance position and width of the $1^2\Pi_u$ resonance state in the Franck–Condon zone. All results have been obtained with the CAP/SAC-CI method using an AUG-cc-pVTZ basis augmented with an even-scaled (4p1d) set. The ranges given are due to different sampling of the "vertical" geometry

	$E_{ m r}$	Γ
Vertical ^a	0.12-0.14	0.002-0.007
Franck–Condon zone ^b	0.09-0.14	0.0003-0.002

^a Range from a set of different equilibrium geometries including experimental, CCSD(T), and B3LYP. ^b Range between the classical turning points along the CC stretch mode using CCSD(T) geometries and normal coordinates.

The second range shows the variation of the resonance parameters along the CC stretch coordinate and the two extreme values correspond to the classical turning points of the neutral NCCN ground state along this mode, which loosely represents the Franck Condon zone. For this choice of sampling, the variations are as expected larger: the resonance position varies by a factor of 1.5, and the width varies by an order of magnitude. Thus, the CAP method predicts a sharp resonance very close to threshold. The particular resonance parameters depend strongly on the specific geometry considered, and consequently, we do not predict a single vertical value. Instead the ranges in Table 4 offer a better sense of the resonance position and width in the Franck Condon zone.

The cross section predicted by the pseudodiholgen model (Fig. 5) is – as expected – unable to describe the intricacies of the experimental excitation cross section of the CC stretch mode. In a sense, the model accounts for the contributions of the CC-stretch mode, while the experimental signal consists of contributions from all modes superimposed on the threshold peak. In other words, the calculated spacing must correspond to the anion C–C stretch frequency (105 meV) and its intensity pattern is governed by a product of two Franck–Condon-like factors as well as an energy-depend switching function that quickly increases from zero at threshold to one at the third vibrational peak (see discussion in the ESI†).

In a favorable light, it may then be possible to associate the predicted peak at 210 meV with the shoulder in the experimental signal that represents a peak upon subtraction of the threshold peak. Similarly, the calculated peak at 105 meV may be entirely hidden in the experimental threshold signal. For the computed 315 meV peak the situation is more murky because the experiment shows peaks at about 305 meV and 360 meV. The most probable explanation in this energy range is coupling to the bending modes resulting in combination modes. But there are clearly far more peaks in the experimental spectrum than excitations directly associated with the CC-stretch are able to explain, and models including one or both bends will likely be needed to account for the boomerang structure.

Still, one important conclusion can be drawn from the computed cross section. While the vertical ranges in Table 4 suggest that the highest peak should occur in the 100 to 120 meV energy region, a suitable vibrational analysis reveals an intensity pattern with a central highest peak at 210 meV and both the 105 and the 315 meV peak are predicted to have almost the same intensity (the 315 meV peak is slightly more intense). Thus, we can only repeat that vertical values of a few tenth of an eV from threshold should be approached with caution. Both the precision of the *ab initio* method and shifts revealed by a subsequent vibrational analysis are in this order of magnitude.

5 Conclusions

In conclusion, we probed the resonances in electron collisions with cyanogen, an important astrophysical molecule. Four pronounced resonances are visible in the experimental cross sections for vibrational excitation. We assign them to the formation of $1^2\Pi_u$ (center at 0.360 eV), $^2\Sigma_u$ (4.1 eV), $^2\Pi_g$ (5.3 eV) and $^2\Sigma_g$ (7.3 eV) shape resonances. The regularized analytical continuation method reproduces the positions of the three lowest resonances very well. Additionally, it provides information about core-excited resonances, which typically do not decay into vibrationally excited states of the target molecule and are thus invisible in the present experiment.

Motivated by the experimental boomerang structure visible in the region of the lowest $1^2\Pi_u$ resonance, we have additionally constructed a one-dimensional pseudodihalogen-like model focusing on the CC stretch vibrational coordinate. This model is designed to predict the direct contribution of the CC-stretch to the CC-stretch excitation curve. It reveals that the experimental spectrum is much richer and that coupling with the bending modes must occur on the timescale of the scattering event. Still, the primitive pseudodihalogen model shows that vertical energies should be taken with a grain of salt, and serve as a first stepping stone to better models that need to include, on the one hand, a virtual state to describe the threshold region, and, on the other hand, at least one additional bending mode giving rise to a Renner–Teller system.

Conflicts of interest

There are no conflicts to declare.

Acknowledgements

This work has been supported by the projects 20-11460S (J. F.) and 18-02098S (R. Č.) of the Czech Science Foundation. T. S. gratefully acknowledges support from the National Science Foundation under Grant No. 1856775. M. E. acknowledges Grants from the Japanese Society for the Promotion of Science (Grant numbers JP16H06511 and JP20H02718).

References

- 1 R. I. Kaiser and A. M. Mebel, *Chem. Soc. Rev.*, 2012, 41, 5490–5501.
- 2 M. Agundez, N. Marcelino and J. Cernicharo, *Astrophys. J., Lett.*, 2018, **861**, L22(1–5).
- 3 T. J. Millar, C. Walsh and T. A. Field, *Chem. Rev.*, 2017, **117**, 1765–1795.
- 4 N. J. Mason, B. Nair, S. Jheeta and E. Szymanska, *Faraday Discuss.*, 2014, **168**, 235–247.
- 5 P. Thaddeus, C. A. Gottlieb, H. Gupta, J. Cernicharo, S. Brunken, M. C. McCarthy, M. Agundez, M. Guelin and J. Cernicharo, *Astrophys. J.*, 2008, 677, 1132–1139.
- 6 M. Agundez, J. Cernicharo, M. Guelin, C. Kahane, E. Roueff, J. Klos, F. J. Aoiz, F. Lique, N. Marcelino, J. R. Goicoechea, M. Gonzales-Garcia, C. A. Gottlieb, M. C. McCarthy and P. Thaddeus, *Astron. Astrophys.*, 2010, 517, L2.
- 7 A. J. Coates, F. J. Crary, G. R. Lewis, D. T. Young, J. H. Waite and E. C. Sittler, *Geophys. Res. Lett.*, 2007, 34, L22103.

- 8 V. Vuitton, P. Lavvas, R. V. Yelle, M. Galand, A. Wellbrock, G. R. Lewis, A. J. Coates and J.-E. Wahlund, *Planet. Space Sci.*, 2009, 57, 1558–1572.
- V. G. Kunde, A. C. Aikin, R. A. Hanel, D. E. Jennings,
 W. C. Maguire and R. E. Samuelson, *Nature*, 1981, 292,
 686–688.
- 10 M. Agundez, J. Cernicharo and P. de Vincente, *et al.*, *Astron. Astrophys.*, 2015, **579**, L10(1–4).
- 11 M. Nsangou, M. Senent and M. Hochlaf, *Chem. Phys.*, 2009, 355, 164–168.
- 12 L. Ng, V. Balaji and K. D. Jordan, Chem. Phys. Lett., 1983, 101, 171.
- 13 A. Kühn, H.-P. Fenzlaff and E. Illenberger, *Chem. Phys. Lett.*, 1987, **135**, 335–339.
- 14 M. Tronc and R. Azria, Chem. Phys. Lett., 1982, 85, 345-349.
- 15 P. Nag, M. Polášek and J. Fedor, Phys. Rev. A, 2019, 99, 052708.
- 16 F. Sebastianelli, F. Carelli and F. Gianturco, *Chem. Phys.*, 2012, 398, 199–2015.
- 17 S. E. Michelin, A. S. Falck, K. T. Mazon, J. J. Piacentini, M. A. Scopel, L. S. S. da Silva, H. L. Oliveira, M. M. Fujimoto, I. Iga and M.-T. Lee, *Phys. Rev. A: At., Mol., Opt. Phys.*, 2006, 74, 022702(1–8).
- 18 G. Brauer, *Handbook of Preparative Inorganic Chemistry*, Academic Press, New York, 2nd edn, Vol. I, 1963, pp. 658–662.
- 19 G. B. Fish, G. J. Cartwright, A. D. Walsh and P. A. Warsop, J. Mol. Spectrosc., 1972, 41, 20–32.
- 20 M. Allan, J. Electron Spectrosc. Relat. Phenom., 1989, 48, 219–351.
- 21 M. Allan, Phys. Rev. Lett., 2007, 98, 123201.
- 22 C. S. Anstöter, G. Mensa-Bonsu, P. Nag, M. Ranković, T. P. R. Kumar, A. N. Boichenko, A. V. Bochenkova, J. Fedor and J. R. R. Verlet, *Phys. Rev. Lett.*, 2020, 124, 203401.
- 23 M. Allan, O. May, J. Fedor, B. C. Ibănescu and L. Andric, Phys. Rev. A, 2011, 83, 052701.
- 24 M. Ranković, P. Nag, M. Zawadzki, L. Ballauf, J. Žabka, M. Polášek, J. Kočišek and J. Fedor, *Phys. Rev. A*, 2018, 98, 052708.
- 25 J. Horáček, I. Paidarová and R. Čurík, J. Chem. Phys., 2015, 143, 184102.
- 26 R. Čurík, I. Paidarová and J. Horáček, *Eur. Phys. J. D*, 2016, 70, 146.
- 27 V. I. Kukulin, V. M. Krasnopolsky and J. Horáček, *Theory of Resonances: Principles and Applications*, Kluwer Academic Publishers, Dordrecht/Boston/London, 1988.
- 28 J. Horáček, P. Mach and J. Urban, *Phys. Rev. A: At., Mol., Opt. Phys.*, 2010, **82**, 032713.
- 29 J. Horáček, I. Paidarová and R. Čurík, J. Phys. Chem. A, 2014, 118, 6536–6541.
- 30 T. Sommerfeld and M. Ehara, *J. Chem. Phys.*, 2015, **142**, 034105.
- 31 A. F. White, M. Head-Gordon and C. W. McCurdy, *J. Chem. Phys.*, 2017, **146**, 044112.
- 32 T. Sommerfeld, J. B. Melugin, P. Hamal and M. Ehara, J. Chem. Theory Comput., 2017, 13, 2550–2560.
- 33 R. Čurík, I. Paidarová and J. Horáček, *Phys. Rev. A*, 2018, **97**, 052704.

PCCP

- 34 P. J. Knowles, C. Hampel and H. Werner, J. Chem. Phys., 1993, 99, 5219-5227.
- 35 M. J. Deegan and P. J. Knowles, Chem. Phys. Lett., 1994, 227, 321-326.
- 36 H. J. Werner, P. J. Knowles, R. Lindh, F. R. Knizia, F. R. Manby, M. Schütz, et al., MOLPRO, version 2010.1, a package of ab initio programs, 2010.
- 37 T. H. Dunning, J. Chem. Phys., 1989, 90, 1007-1023.